JOURNAL OF Materials CHEMISTRY

Investigation on lanthanide-doped Y_2O_3 nanopowders obtained by wet chemical synthesis

Stefano Polizzi,*[a] Marino Battagliarin,[a] Marco Bettinelli,[b] Adolfo Speghini[b] and Giuliano Fagherazzi[a]

[a]*Dipartimento di Chimica Fisica, Università Ca' Foscari di Venezia, Via Torino 155/b, I-30170 Mestre-Venezia, Italy. E-mail: polizzi@unive.it*
[b]*Dipartimento Scientifico e Tecnologico, Università di Verona, Strada le Grazie 15, I-37134 Verona, Italy*

Received 13th July 2001, Accepted 12th December 2001
First published as an Advance Article on the web 29th January 2002

Trivalent europium or erbium doped yttria samples obtained by a wet chemical synthesis procedure have been investigated by wide and small angle X-ray scattering, scanning and transmission electron microscopy and luminescence spectroscopy. On the micron scale the powders obtained are large, compact aggregates built up of platelets about 200 nm large and 10 nm thick, arranged with some degree of order. Platelets are nanocrystals with the cubic structure of yttria and contain randomly distributed pores of 2–4 nm at average distance of about 10 nm. Lanthanide dopants have no noticeable effect on the morphology but cause the lattice parameter of the yttria structure to change in a way proportional to their ionic radius. The luminescence spectrum in the visible region of the Eu^{3+} doped nanocrystals indicates the presence of a high degree of disorder in the environment around the lanthanide ion.

Introduction

In recent years, numerous investigations have dealt with cubic Y_2O_3 doped with Eu^{3+} ions, which is one of the most efficient red emitting phosphors in fluorescence lamps.[1,2] The optical and electronic properties of nanocrystalline materials differ from those of the bulk samples and can be influenced by the particle size.[3–5] Moreover, the advances made in the size reduction of electronic devices require the investigation of the physical properties of materials with particle size in the nanometer range.

Many techniques have been employed to prepare nanosized yttria doped with lanthanide ions, as for instance pulsed laser deposition,[6–8] combustion,[9] propellant[10] or wet chemical[11] synthesis. In some recent publications, we have reported on the structure of lanthanide-doped yttria samples obtained by propellant synthesis[12,13] and on the spectroscopy of Er^{3+} doped yttria obtained by this method.[14] This method gives rise to nanopowders, which aggregate to build up a very porous, sponge-like microstructure with mass-fractal scaling properties. In the present paper, we focus on the structure, morphology and luminescence of similar samples obtained by a wet chemical synthesis, which is based on a gel solution.[11] Both methods are able to produce powders with nanometric structures, which give them interesting optical properties. On the contrary, their structure in the micrometer scale is completely different, suggesting different final applications of these materials. The Eu^{3+} ion can be usefully employed as a spectroscopic probe of the local structure of the sites accommodating Ln^{3+} ions in solids.[15] The luminescence properties in the visible region of the Eu^{3+} doped nanoparticles are reported, and their differences with respect to Eu^{3+} doped yttria samples prepared by conventional ceramic synthesis are described and discussed.

Materials and methods

Samples

Er^{3+} and Eu^{3+} doped yttria samples were obtained using a wet synthesis procedure[16] reacting an alcoholic solution containing $Y(NO_3)_3$ (Aldrich, 99.9%) and $Er(NO_3)_3$ (Aldrich, 99.9%) or $Eu(NO_3)_3$ (Aldrich, 99.9%) with a solution of a surface modifier (β-alanine + Tween 80 in 1 : 1 weight ratio) at pH > 10. The two solutions were mixed and the resulting gel was centrifuged for 1 h at 3000 rpm. After removing the aqueous solution, the powder was dried at 70 °C for 24 h and then heat treated in a muffle for 12 h at 500 °C. Undoped yttria samples were obtained following the same preparation procedure. The specific surface was determined by using the BET method, and found to be 19 $m^2\ g^{-1}$.

For comparison purposes, bulk $Y_{2-x}Eu_xO_3$ ($x = 0.02, 0.2$) samples were prepared by intimately mixing Y_2O_3 (Aldrich, 99.99%) and Eu_2O_3 (Aldrich, 99.999%), pressing the powders into pellets under 20 t and firing them at 1500 °C for 48 h.

SEM and TEM

SEM images were taken with a Jeol (Tokyo, Japan) JSM 5600 LV equipped with an Oxford Instrument (Oxford, England) 6587 EDS microanalysis detector. Samples were coated with a Pd/Au thin film, in order to avoid charging effects.

TEM images were taken with a Jeol 3010, operating at 300 kV, equipped with a Gatan (Warrendale, PA, USA) slow-scan CCD camera (Mod. 794) and an Oxford Instrument (Oxford, England) EDS microanalysis detector (Mod. 6636). The powder was dispersed in an isopropyl alcohol solution and deposited on a holey carbon film.

WAXS

A Philips X'Pert vertical goniometer with Bragg–Brentano geometry, connected to a highly stabilized generator, was used for XRD analysis. Cu-K_α Ni-filtered radiation, a graphite monochromator on the diffracted beam and a proportional counter with pulse height discriminator were used. Measurements in a 14°–140° range were taken with a step size of 0.05° and 10 s per point. For line broadening analysis data were collected on limited ranges around the peaks of interest for five

 DOI: 10.1039/b106240a

runs of 10 s per point each and then averaged. The step size was 0.05°, except for the 222 reflection, where 0.02° was used.

Unit cell-edge values were calculated by using the angular peak position of ten to fifteen reflections in the 2θ range 25°–85° (2θ is the scattering angle). The cell-edge value was extrapolated using a least-square fit in the diagram reporting cell-edge values calculated with the position of each single reflection as a function of $\cos\theta\mathrm{cotg}\theta$.[17,18] Peak positions were obtained by previously reported best-fitting procedures,[19,20] where each peak is described by a couple of constrained pseudo-Voigt functions ($K_{\alpha 1}$ and $K_{\alpha 2}$ profiles) and the background by a polynomial function.

Line broadening analysis was carried out by Warren–Averbach analysis[21,22] using the best-fitted pseudo-Voigt functions for the 222/444 and 400/800 couples of reflections. This method allows one to obtain average crystallite sizes, as well as average r.m.s. microstrains, conventionally determined at half average crystallite size. Instrumental broadening is analytically deconvolved by using the Fourier transform.[17]

SAXS

Measurements were made using a Kratky (PAAR) camera with an entrance slit of 25 μm. Nickel-filtered Cu K_α radiation, a pulse-height discriminator and a proportional counter were used in the preset counting mode (1.6×10^4 counts per angular step) of data collection. Experimental intensities, $J(h)$, were corrected for absorption and air scattering ($h = 4\pi\sin\theta/\lambda$, λ is the radiation wavelength). In order to deconvolve intensities from the shape of the primary beam (desmearing), the Du Mond method was used[23,24] which is rigorously valid for a primary beam of infinite height and constant intensity, following the same procedure as in ref. 25 and 26.

Measurements with pinhole geometry were carried out using synchrotron radiation at HASYLAB (DESY) in Hamburg. The high resolution beamline (USAXS at BW4) was used at 14 keV and 8.9 keV with sample-detector distance of 3.9 m and 12.6 m, respectively.

Luminescence spectra

The 488.0 nm line of an Argon laser (mod. 2017, Spectra Physics) was used to excite room temperature luminescence spectra. A fiber optic probe was employed. The scattered signal was analyzed by a half-metre monochromator and a CCD detector (Spectrum One, Jobin–Yvon). A 1200 lines mm^{-1} grating was used to collect high resolution (≈ 1 cm^{-1}) luminescence spectra in the region of the $^5D_0 \rightarrow {}^7F_0$ transition of Eu^{3+}, whilst the other laser-excited luminescence spectra were measured using a 150 lines mm^{-1} grating.

Results and discussion

In Fig. 1 the SEM image of an yttria sample prepared by wet synthesis (a) is compared with one of a similar sample obtained by propellant synthesis (b) on the micrometer scale. The different surface structure can be clearly seen: the sample in (b) has a very open, sponge-like microstructure in contrast with the compact surface in (a) (brighter areas in (a) are due to a small charging of some on-top aggregates). Furthermore, samples prepared by propellant synthesis showed a similar morphology over a large range of magnifications, which is due to their fractal structure. On the contrary, further magnifications of samples prepared by wet synthesis disclose a completely different underlying morphology. Fig. 2 shows higher magnifications of the area enclosed in the white frame in Fig. 1. At this sub-micrometre scale the compact structure is revealed to be an aggregate of platelets about 200 nm large and 10 nm thick, arranged with some degree of orientation. In the sample area shown in Fig. 2 most of the platelets are roughly oriented

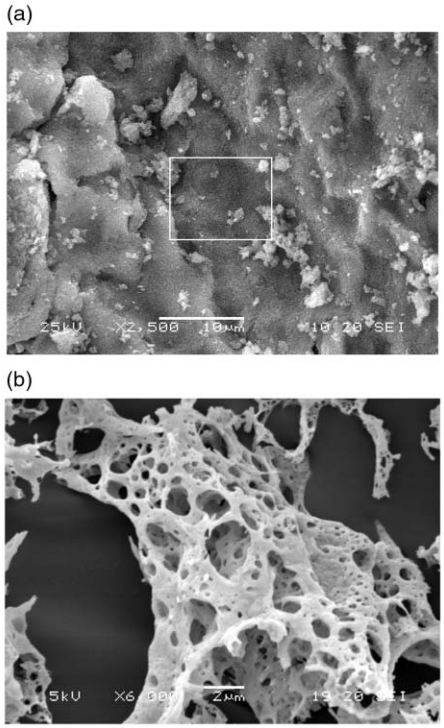

Fig. 1 SEM image of an yttria sample obtained by wet synthesis (a) compared with an yttria sample prepared by propellant synthesis (b) (scale bar in (a): 10 μm; in (b) 2 μm).

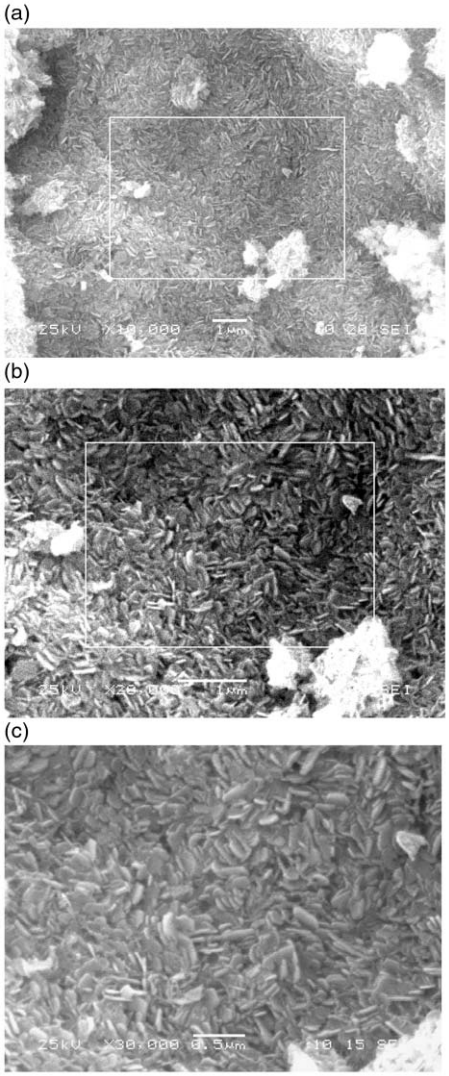

Fig. 2 Higher magnifications of the area in the white frame of Fig. 1(a) (SEM images) (scale bar in (a) and (b): 1 μm; in (c) 0.5 μm).

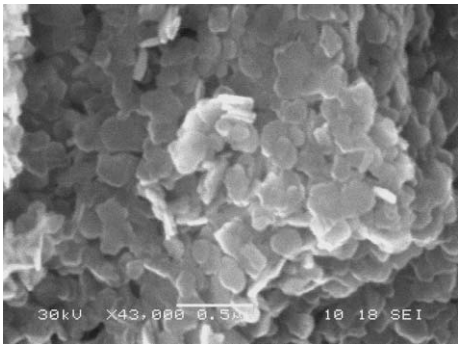

Fig. 3 SEM image of a different region of the yttria sample with a ''top-view' of the platelets (scale bar: 0.5 μm).

perpendicular to the surface of the agglomerate, but in other parts of the sample they lay more parallel to the surface (Fig. 3). Platelets have irregular shapes, but there seems to be a roughly rounded basic unit that can merge together to give rise to larger particles. In some area of the sample, platelets as large as 1–2 μm have been also found (not shown).

Platelets have an inner structure, which becomes apparent by further magnifications. In Fig. 4(a) a small agglomerate of platelets is shown, as seen using a TEM. In Fig. 4(b) the area enclosed in the white frame is enlarged: few platelets are seen ''top-view' and one is seen ''side-view'. The latter is further magnified in Fig. 4(c), where fringes separated by 0.30 nm and parallel to the platelet surface become visible; these fringes are due to the (222) crystal planes of the cubic structure of yttria. The top-view platelets show a non-uniform density, which is more clearly seen in Fig. 5(a), where an isolated platelet is shown: at the nanometer scale platelets have a porous structure, with pores of about 2–4 nm randomly distributed inside the platelets. At higher magnifications (Fig. 5(b), (c)),

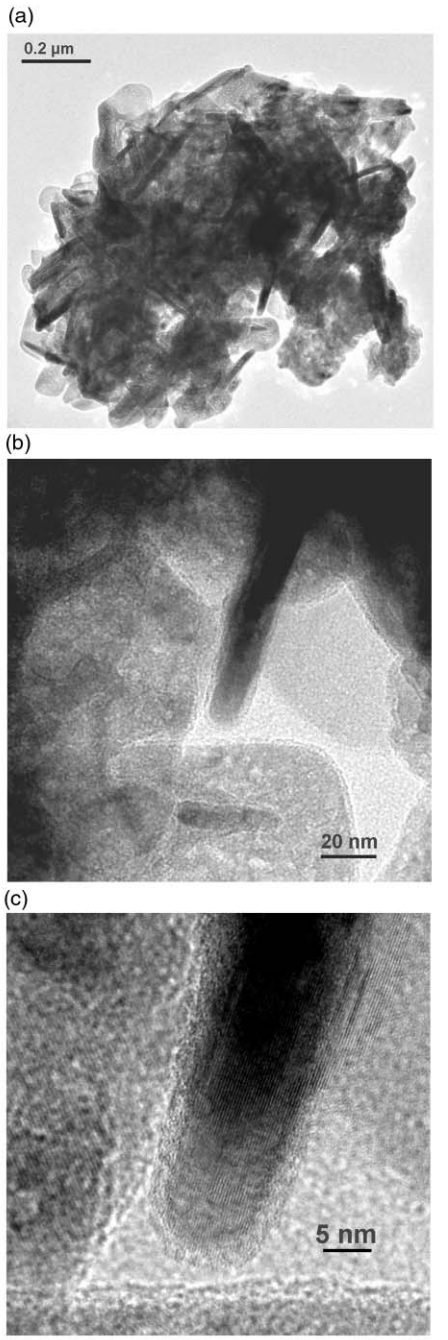

Fig. 4 TEM image of an agglomerate of platelets (a) and magnifications of the area in the white frame ((b) and (c)).

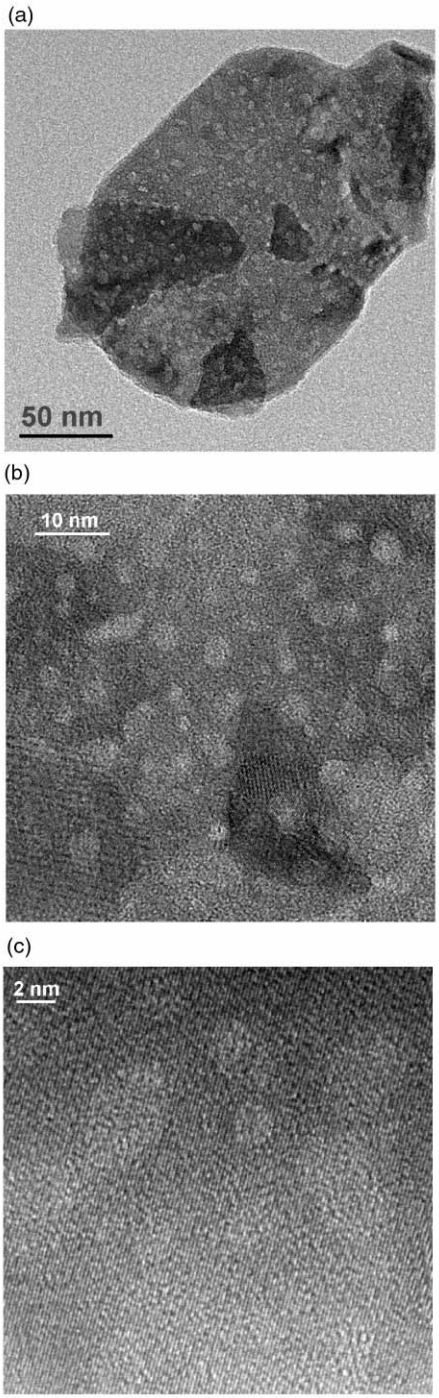

Fig. 5 TEM image of an isolated platelet (a) and high resolution images of one region inside it (b) and (c).

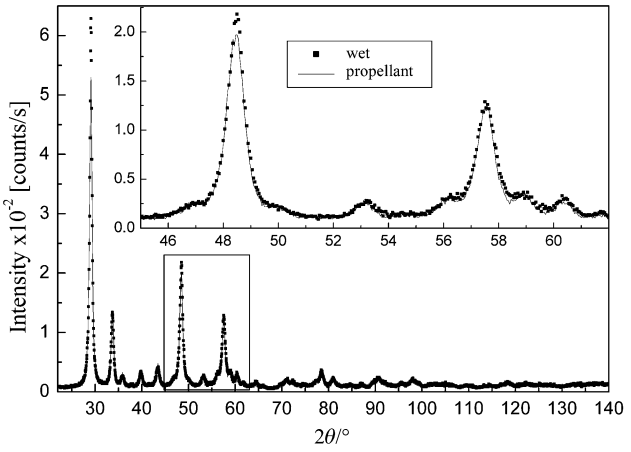

Fig. 6 Comparison of X-ray diffraction spectra of yttria samples prepared by wet synthesis (square symbols) and by propellant synthesis (solid line).

fringes separated by 0.19 nm become visible over the whole area of the image; these fringes are due to the (440) crystal planes. As can be seen also in Fig. 5(a), not all of the material forms such well-shaped platelets; many smaller and irregularly shaped fragments (darker regions in Fig. 5(a)) and some larger pieces of material are present. All yttria samples show similar micro-and nanostructures regardless of the presence of dopants.

WAXS diffractograms (Fig. 6) confirmed that all samples prepared by wet synthesis are made up of a single crystalline phase and that no significant amorphous material is present. Samples have the cubic structure of yttria (space group: $Ia\bar{3}$),[27] with a lattice parameter which, for the doped samples, is found to vary with the ionic radii of the dopant (see Table 1) in the same linear way that was found for samples obtained by propellant synthesis.[13] No preferential orientation was found. Line broadening analysis of the diffraction peaks indicated a volume-weighted average size of the coherently diffracting domains of the order of 10 nm in both investigated crystallographic directions (see Table 1) and negligible values for the average r.m.s. microstrains. In fact, in spite of the very different morphology and nanostructure, diffractograms are almost identical to the one of the corresponding samples prepared by propellant synthesis. However, TEM suggests that, while the crystalline peaks of the samples prepared by propellant synthesis are due to nanocrystallites of the order of 10 nm, those of samples obtained by wet synthesis are due to larger nanocrystals where an average coherence length of about 10 nm is caused by the presence of the pores. In fact, the peak broadening gives in this case a measure of the average distance between pores, which in the TEM images (see Fig. 5) appears to be slightly smaller due to the projection of the sample volume in two dimensions, which is a characteristic of this technique.

In contrast with the WAXS diffractograms, the SAXS data reveal the morphological difference of the samples obtained by the two different preparation methods. Fig. 7 shows the SAXS desmeared intensities of yttria nanosized powders prepared by

Table 1 Cell-edge values, *a*, obtained by Wagner method and crystallite dimensions obtained by Warren–Averbach method for two different couples of WAXS reflections. The found average r.m.s. microstrains are negligible

Sample	*a*/nm	$<D_v>$/nm 222/444	400/800
Y_2O_3	1.0613(3)	13	11
$Y_{1.8}Eu_{0.2}O_3$	1.0644(4)	11	11
$Y_{1.8}Er_{0.2}O_3$	1.0609(4)	13	12

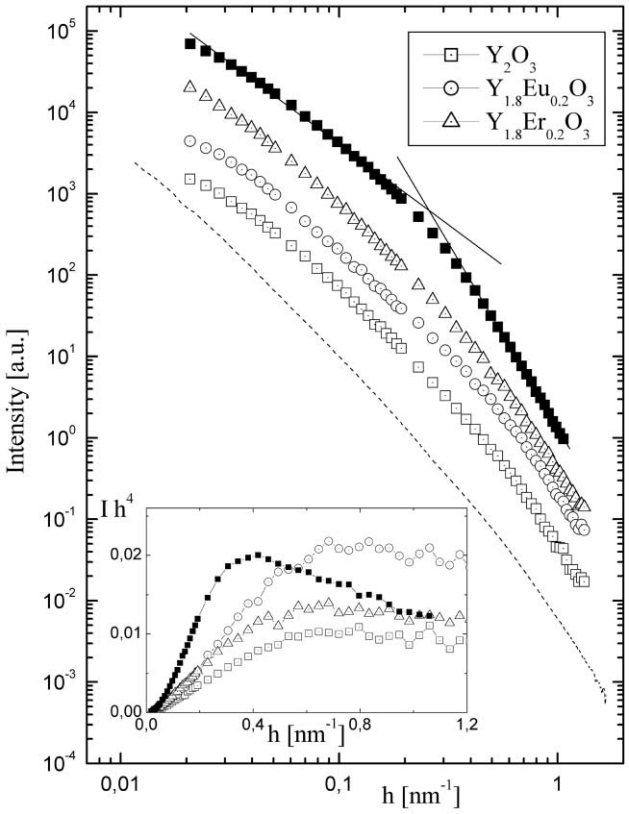

Fig. 7 SAXS data of yttria-based nanosized powders obtained by wet synthesis, compared with an un-doped sample obtained by propellant synthesis (solid symbols). The shown intensities were obtained by desmearing the data collected by using a Kratky camera. The dashed line is relevant to the measurement made using a pin-hole instrument with synchrotron radiation of the un-doped sample obtained by wet synthesis. Inset: Porod plot of the data obtained by the Kratky camera.

wet chemical method on a double logarithmic plot and, for comparison, the data of a sample obtained by propellant synthesis (solid squares). While propellant samples show two slopes with a crossover,[12,13] a trend which is characteristic of a mass-fractal structure, the data relevant to samples prepared by wet chemical method have a continuously changing slope. The difference in the trend of the data relevant to the two preparation methods is further amplified in the Porod plot, *i.e.*, $I(h)h^4$ *versus* *h*, shown in the inset. In order to check for possible artifacts introduced by the desmearing procedure, a measurement was made for one of the samples with a pin-hole geometry, confirming the same trend over a larger *h*-range (see Fig. 7). Apparently, the scattering of the different structural features evidenced by electron microscopy (pores, fragments, platelets, aggregates) overlaps on the different scales to give a continuous variation in the scattering, yet without the precise auto-scaling property of fractals. The particular slope (steeper than −4) found by us in the high *h*-range for samples prepared by propellant synthesis (doped and un-doped) is not present in the samples prepared by wet synthesis. These samples show the classical Porod regime (−4 slope), which indicates the presence of a smooth particle surface where a drastic change of electron density occurs.

Luminescence spectra measured with a conventional spectrofluorimeter of nanocrystalline Eu^{3+} doped yttria obtained by the method employed in this study have already been reported,[11,15,28] but not thoroughly discussed.

The room temperature laser-excited luminescence spectra of the $Y_{1.98}Eu_{0.02}O_3$ samples prepared by wet chemical and conventional solid-state synthesis, measured with an excitation wavelength of 488.0 nm, are shown in Fig. 8. The spectra

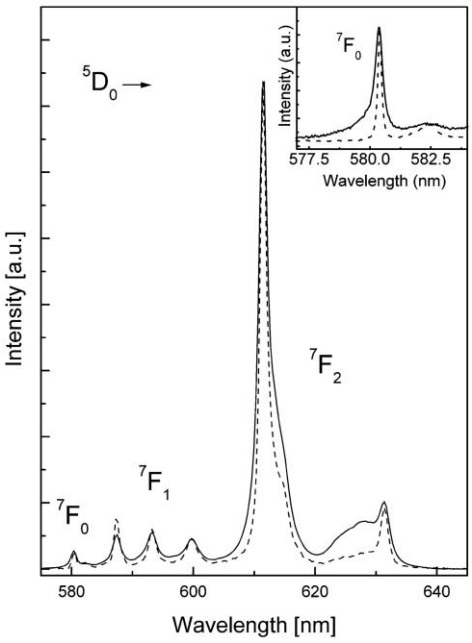

Fig. 8 Room temperature luminescence spectra of Eu^{3+} doped yttria prepared by wet chemical synthesis (solid line) and by conventional solid state reaction (dashed line).

consist of $f \rightarrow f$ emission transitions from the $^5D_0$ excited state to the ^7F_J (J = 0,1,2,3) multiplet of the Eu^{3+} ion. The measured luminescence spectrum of the nanoparticles is similar to that obtained by Sharma *et al.*,[11] although the resolution of the latter is limited by the use of a conventional spectrofluorimeter, so that a detailed comparison between the two spectra cannot be made. The cubic Y_2O_3 lattice has two different sites for Eu^{3+} substitution, with point-group symmetry C_2 and C_{3i}, respectively.[29] According to the selection rules, the electric dipole transitions for the Eu^{3+} ions occupying the C_2 sites are allowed, while those for the Eu^{3+} ions in C_{3i} sites are forbidden. The band at 580.4 nm observed for the $^5D_0 \rightarrow {}^7F_0$ transition is attributed to Eu^{3+} ions in sites of C_2 symmetry (see inset of Fig. 8). The weak band at 582.4 nm can be identified as the $^5D_0 \rightarrow {}^7F_{1a}$ magnetic dipole transition of Eu^{3+} ions in sites of C_{3i} symmetry, following the assignment made in many previous studies,[30–33] also on the basis of site selection experiments The band due to the $^5D_0 \rightarrow {}^7F_{1b}$ magnetic dipole transition is partially superimposed to the stronger bands due to the $^5D_0 \rightarrow {}^7F_1$ transitions of Eu^{3+} ions in sites of C_2 symmetry, making its identification and assignment not possible in the present experimental conditions. In general, the peak positions of the bands of the luminescence spectra are very similar for the bulk and nanocrystalline samples. Nonetheless, it is evident from Fig. 8 that all the bands of the sample prepared by wet synthesis are broader with respect to the bulk sample, denoting a higher disorder of the crystalline environment of the Eu^{3+} ions in the nanoparticles. Moreover, the ratio of the integrated intensities of the $^5D_0 \rightarrow {}^7F_2$ and $^5D_0 \rightarrow {}^7F_1$ transitions

$$R = \frac{I(^5D_0 \rightarrow {}^7F_2)}{I(^5D_0 \rightarrow {}^7F_1)} \quad (1)$$

can be considered indicative of the asymmetry of the average coordination polyhedron of the Eu^{3+} ion.[34] The R values observed for the bulk and nanocrystalline $Y_{1.98}Eu_{0.02}O_3$ samples are 5.3 ± 0.1 and 6.5 ± 0.1, respectively. The higher R value obtained for the nanoparticles suggests that on the average the local environment of the Eu^{3+} ions is more distorted. This is attributed to the higher number of Eu^{3+} ions near or at the surface of the particles due to the higher surface/volume ratio of the nanosized material. This result is in agreement with the aforementioned observed higher inhomogeneous broadening for the nanocrystalline sample.

Conclusions

The micro-and nanostructure of an yttria material prepared by a wet synthesis method, have been characterized by different investigation techniques. This preparation method allows one to easily dope the yttrium oxide with lanthanide elements, in order to obtain materials for electroluminescent applications. Samples have shown to be built up of crystalline platelets with a porous structure at the nanometre scale, which forms large, partially ordered aggregates on the micrometre scale. The luminescence spectroscopy of the Eu^{3+} doped nanocrystalline samples obtained by wet chemical methods are substantially similar to the ones typical of bulk cubic Eu^{3+} doped yttria, but are characterized by a markedly higher inhomogeneous broadening, caused by disorder at the Eu^{3+} sites. The spectra also indicate that these sites are more distorted compared to bulk yttria. A detailed analysis of the optical spectroscopy of nanocrystalline Eu^{3+} and Er^{3+} doped yttria will be reported in future papers.

Although X-ray diffraction indicates the same particle size (10 nm) as for Y_2O_3 obtained by solution combustion synthesis, the underlying morphology and nanostructure is completely different. We found porous single-crystal platelets of about 200 nm × 10 nm. Pores interrupt the coherence length along the platelets, giving rise to the misleading 10 nm value, which represents in this case the distance between pores and not the size of the platelets.

Acknowledgement

For the X-ray measurements, the technical assistance of T. Finotto of the Ca' Foscari Venice University's Department of Physical Chemistry is greatly acknowledged. We also thank Dr. G. von Krosigk for technical assistance at DESY. This project was funded by the 1999 PRIN/Cofin contract of the Italian Ministry for University and Research (MURST) and supported by the TMR-Contract ERBFMGECT950059 of the European Community.

References

1 G. Blasse and B. C. Grabmeier, *Luminescent Materials*, Springer, Berlin, 1994.
2 C. R. Ronda, *J. Lumin.*, 1997, **72**, 49.
3 R. N. Bhargava, D. Gallagher, X. Hong and A. Nurmikko, *Phys. Rev. Lett.*, 1994, **72**, 416.
4 P. Alivisatos, *Science*, 1996, **271**, 933.
5 T. Goldburt, B. Kulkarni, R. N. Bhargava, J. Taylor and M. Libera, *J. Lumin.*, 1997, **72–74**, 190.
6 H. Eilers and B. M. Tissue, *Chem. Phys. Lett.*, 1996, **251**, 74.
7 D. K. Williams, B. Bihari, B. M. Tissue and J. M. McHale, *J. Phys. Chem B*, 1998, **102**, 916.
8 B. M. Tissue, *Chem. Mater.*, 1998, **10**, 2837.
9 L. E. Shea, J. McKittrick, O. A. Lopez and E. Sluzky, *J. Am. Ceram. Soc.*, 1996, **79**, 3257.
10 G. Tessari, M. Bettinelli, A. Speghini, D. Ajò, G. Pozza, L. E. Depero, B. Allieri and L. Sangaletti, *Appl. Surf. Sci.*, 1999, **144–145**, 686.
11 P. K. Sharma, M. H. Jilavi, H. Schmidt and V. K. Varadan, *Int. J. Inorg. Mater.*, 2000, **2**, 407.
12 G. Fagherazzi, S. Polizzi, M. Bettinelli and A. Speghini, *J. Mater. Res.*, 2000, **15**, 586.
13 S. Polizzi, G. Fagherazzi, M. Battagliarin, M. Bettinelli and A. Speghini, *J. Mater. Res.*, 2001, **16**, 146.
14 J. A. Capobianco, F. Vetrone, T. D'Alesio, G. Tessari, A. Speghini and M. Bettinelli, *Phys. Chem. Chem. Phys.*, 2000, **2**, 3203.
15 J.-C. G. Bünzli, in *Lanthanide Probes in Life, Chemical and Earth Sciences: Theory and Practice*, ed. J.-C. G. Bünzli and G.R. Choppin, Elsevier, Amsterdam, 1989, p. 219.
16 K. Sharma, R. Nass and H. Schmidt, *Opt. Mater.*, 1998, **10**, 161.
17 C. N. J. Wagner, in *Local Atomic Arrangements Studied by X-ray*

Diffraction, *Metals Society Conference*, ed. J.B. Cohen and J.E. Hilliard, Gordon & Breach, New York, 1966, vol. 36, p. 219.
18 P. I. Adler and C. N. J. Wagner, *J. Appl. Phys.*, 1962, **33**, 3451.
19 S. Enzo, S. Polizzi and A. Benedetti, *Z. Kristallogr.*, 1985, **170**, 275.
20 S. Enzo, G. Fagherazzi, A. Benedetti and S. Polizzi, *J. Appl. Cryst.*, 1998, **21**, 536.
21 E. Warren and B. L. Averbach, *J. Appl. Phys.*, 1950, **21**, 595.
22 E. Warren and B. L. Averbach, *J. Appl. Phys.*, 1952, **23**, 497.
23 J. W. M. Du Mond, *Phys. Rev.*, 1947, **72**, 83.
24 A. Guinier and G. Fournet, *Small-Angle Scattering of X-rays*, Wiley, New York, 1955, p. 116.
25 P. Guinier, *C. R. Hebd. Seances Acad. Sci.*, 1939, **208**, 894.
26 P. Guinier and G. Fournet, *Small-Angle Scattering of X-rays*, Wiley, New York, 1955, p. 25.
27 *Powder Diffraction File*, JCPDS International Centre for Diffraction Data, Swarthmore PA, PDF n. 43–1036.
28 P. K. Sharma, M. H. Jilavi, R. Nass and H. Schmidt, *J. Lumin.*, 1999, **82**, 187.
29 N. C. Chang, *J. Appl. Phys.*, 1963, **34**, 3500.
30 J. Heber, K. H. Hellwege, U. Köbler and H. Murmann, *Z. Physik*, 1970, **237**, 189.
31 R. Pappalardo and R. B. Hunt Jr., *J. Electrochem. Soc.*, 1985, **132**, 721.
32 J. B. Gruber, R. P. Leavitt, C. A. Morrison and N. C. Chang, *J. Chem. Phys.*, 1985, **82**, 5373.
33 T. Igarashi, M. Ihara, T. Kusunoki, K. Ohno, T. Isobe and M. Senna, *Appl. Phys. Lett.*, 2000, **76**, 1549.
34 W. J. L. Oomen and A. M. A. van Dongen, *J. Non-Cryst. Solids*, 1989, **111**, 205.